mathematics

Article

Distributed Interval Observers with Switching Topology Design for Cyber-Physical Systems

Junchao Zhang, Jun Huang * and Changjie Li

The School of Mechanical and Electrical Engineering, Soochow University, Suzhou 215325, China; 2129402025@stu.suda.edu.cn (J.Z.); 20225229049@stu.suda.edu.cn (C.L.)
* Correspondence: jhuang@suda.edu.cn

Abstract: In this paper, the distributed interval estimation problem for networked Cyber-Physical systems suffering from both disturbances and noise is investigated. In the distributed interval observers, there are some connected interval observers built for the corresponding subsystems. Then, due to the communication burden in Cyber-Physical systems, we consider the case where the communication among distributed interval observers is switching topology. A novel approach that combines L_∞ methodology with reachable set analysis is proposed to design distributed interval observers. Finally, the performance of the proposed distributed interval observers with switching topology is verified through a simulation example.

Keywords: cyber-physical systems; distributed interval observers; reachable set analysis; switching topology; L_∞ technique

MSC: 93D05

Citation: Zhang, J.; Huang, J.; Li, C. Distributed Interval Observers with Switching Topology Design for Cyber-Physical Systems. *Mathematics* **2024**, *12*, 163. https://doi.org/10.3390/math12010163

Academic Editor: Sergey Ershkov

Received: 30 November 2023
Revised: 25 December 2023
Accepted: 29 December 2023
Published: 4 January 2024

1. Introduction

Cyber-Physical Systems (CPSs) are the combinations of physical procedures, high-efficiency computation, communication, and effective control defined by [1]. Architecturally, from [2], a typical CPS can be divided into three layers, which are composed of the sensing layer, the network layer, and the control layer. The development of distributed sensing and networking technologies such as [3,4] has enabled omnipresent sensing and computing capabilities. This has led to the implementation of CPSs in large-scale networks. CPSs are widely used in industrial informatics [5] manufacturing [6], healthcare [7], electrical grids [8], and so on. State estimation and observer design are crucial research areas in CPSs. Ref. [9] used a sliding mode observer and integrated the event-triggered mechanism to estimate the state of CPSs from sensor measurements. Ref. [10] introduced a security estimator combined with a Kalman filter to improve the practical performance of state estimation for CPSs. Ref. [11] accomplished state estimation and resilient control of CPSs using finite time observer techniques and switching schemes. It should be noted that the state estimation for CPSs with bounded disturbance and noise has not been investigated sufficiently.

On the other hand, disturbances and noise always exist in real systems, and the interval observer serves as a powerful estimator of upper and lower bounds for uncertain systems with disturbances and noise. In [12], the concept, as well as the framework of interval observer, were presented. Using the monotone system theory, Refs. [13,14] proposed the approach of coordinate transformation that serves as an efficient strategy to reduce the strict conditions for interval observer design. In recent years, the set-membership estimation method was applied effectively in interval observer design. A two-step interval observer design methodology that combines reachability analysis with robust observer was first presented in [15]. In [15], the H_∞ method and reachable set analysis are combined to design interval observers that eliminate the effects of perturbations and noise on the system. At the same time, the L_∞ (or L_2) method is also a powerful, robust property, and it is widely used in control and observation fields, such as [16–18]. It has been recently shown by [19–21] that the reachability analysis estimation method can not only enhance the accuracy of estimation but also increase the design freedom. Concurrently, in the context of distributed systems, several recent studies have been conducted on distributed interval observers, such as [22–24]. Ref. [22] designed distributed interval observers based on the monotone system approach for multiagent systems. Ref. [23] considered a distributed interval observers design problem for a class of linear time-invariant systems with uncertainty. At the same time, Ref. [24] improved distributed interval observers by using a set-membership estimation approach. However, the topology of interval observer in the aforementioned work [22–24] is fixed, and it is usually switching with respect to time in practice.

In light of the above discussion, for the problem of state estimation for uncertain CPSs, we apply distributed interval observers to such systems. Since the state estimation of CPSs with bounded disturbances and noise has not been investigated sufficiently, it is meaningful to study the state estimation problem for uncertain CPSs. Each interval observer has two types of observer gain: one is obtained by using the traditional observer design method, and the other one is determined by employing neighborhood information. Considering the practical communication problem of the network layer in CPSs, we suppose that the communication among distributed interval observers is described by switching topology. There are three main challenges: one is to design L_∞ observers with optimal performance for networked CPSs, another is to construct a reachable set analysis framework for CPSs, which then gives upper and lower bounds on the state of the system, and the last is to solve the switching topology problem among the observers. The contributions of this paper are summarized in aspects below.

(1) A distributed interval observer methodology for CPSs is proposed. Compared with the monotone system method, the estimation accuracy is greatly improved by using the two-step method. The L_∞ technique is used to deal with the effects of uncertainty in observer design.
(2) The switching topology with average dwell time (ADT) among distributed interval observers is taken into account and is more closely aligned with the actual system. It can also reduce the communication burden of CPSs.

This paper is structured as follows, with the rest of the paper starting with the graph theory, system model, and some basics presented in Section 2. In Section 3, the optimal robust observer is designed using the L_∞ technique. In order to complete the interval estimation, a reachability analysis methodology is used to design the distributed interval observer. In Section 4, the paper simulates a networked CPS with four Unmanned Aerial Vehicles (UAV) models to illustrate the effectiveness of the distributed interval observer. Finally, Section 5 concludes the paper.

Notation: For a matrix of real symmetry $E \in R^{N\times N}, E \succ 0$ demonstrates that E is positive definite, while $E \prec 0$ demonstrates that E is negative and $He(E) = E + E^T$. The maximal (minimum) eigenvalue of the matrix Q is denoted by $\lambda_{max}(Q)(\lambda_{min}(Q))$. The norm L_2 of the vector v is represented by $\|v\|_2$. In other words, $\|v\|_2 = \sqrt{v^T v}$. Similarly, the norm L_∞ of the vector v is denoted by $\|v\|_\infty$. The symbol $*$ means the term that can arise due to symmetry in the symmetric matrices.

2. Preliminaries

2.1. Graph Theory

For a digraph G which has N vertices, $\mathcal{A} = [a_{ij}] \in R^{N\times N}$ is called the adjacency matrix. The weight associated with the edge $(i,j) \in S$ that connects node i to node j is called a_{ij}, and $\mathcal{A}$ is provided by $a_{ij} = 0$. The length path from vertex i to vertex j is made up of $t+1$ distinct vertices with consecutive vertices adjacent to each other. If there is a path connecting any two vertices of the graph $\mathcal{G}$, the graph $\mathcal{G}$ is considered connected. $\mathcal{L} = \mathcal{D} - \mathcal{A}$ is defined as Laplacian matrix of a graph $\mathcal{G}$. $\mathcal{D}$ is referred to as a degree matrix of $\mathcal{G}$. The Laplacian matrix $\mathcal{L}$ of a connected graph has a single zero eigenvalue, and 1_N

is the associated eigenvector. Furthermore, $0 = \lambda_1(\mathcal{G}) \leq \cdots \leq \lambda_N(\mathcal{G})$ if $\mathcal{G}$ is connected, where $\lambda_i(\mathcal{G})$ $(i = 1, 2, \cdots, N)$ is the eigenvalue of a Laplacian matrix $\mathcal{L}$.

Lemma 1 ([25])**.** *For a strongly connected graph $\mathcal{G}$, denote $t_i (i = 1, 2, \cdots, N)$ as the left eigenvector with a 0 eigenvalue, and $T = diag\{t_1, t_2, \cdots\cdots, t_N\}$, then, we can obtain $T\mathcal{L} + \mathcal{L}^T T \geq 0$.*

Lemma 2 ([26])**.** *Suppose that graph $\mathcal{G}$ is a strongly connected and balanced graph, and the algebraic connectivity of $\mathcal{G}$ is defined by $a(\mathcal{L}) = \min_{t^T x = 0, x \neq 0} \frac{x^T(T\mathcal{L} + \mathcal{L}^T T)x}{2x^T T x}$ where $T = diag\{t_1, t_2, \cdots\cdots, t_N\}$. Then, we can obtain $a(\mathcal{L}) = \lambda_{min}(\frac{He(\mathcal{L})}{2})$.*

2.2. System Model

For a networked CPS, consider a network with N subsystems. The following is the ith subsystem with disturbances and noise:

$$\begin{aligned} x_i(k+1) &= Ax_i(k) + Bu_i(k) + p_i(k), \\ y_i(k) &= Cx_i(k) + q_i(k), \end{aligned} \tag{1}$$

where $x_i(k) \in R^n$ is the state, $u_i(k) \in R^n$ is the control input, $y_i(k) \in R^m$ is the output, $p_i(k) \in R^n$ is the disturbance, $q_i(k) \in R^m$ is the noise. $A \in R^{n\times n}$, $B \in R^{n\times n}$ and $C \in R^{m\times n}$ are constant matrices.

In the following, it is supposed that the communication topology of the subsystem is strongly connected. The global dynamic system of (1) can be given:

$$\begin{aligned} x(k+1) &= \overline{A}x(k) + \overline{B}u(k) + p(k), \\ y(k) &= \overline{C}x(k) + q(k), \end{aligned} \tag{2}$$

where $x = [x_1^T, \cdots, x_N^T]^T$, $u = [u_1^T, \cdots, u_N^T]^T$, $y = [y_1^T, \cdots, y_N^T]^T$, $q = [q_1^T, \cdots, q_N^T]^T$, $p = [p_1^T, \cdots, p_N^T]^T$, $\overline{A} = diag\{\underbrace{A, \cdots, A}_{N}\}$, $\overline{B} = diag\{\underbrace{B, \cdots, B}_{N}\}$ and $\overline{C} = diag\{\underbrace{C, \cdots, C}_{N}\}$.

Since the information can be received by a single subsystem from its neighborhood, we consider the case of switching topology of the observer system and then present $\phi(k)$, a stepwise constant function that takes values from the finite collection $S = \{1, \quad 2, \quad \cdots, \quad N\}$. The observer dynamics of ith subsystem are:

$$\hat{x}_i(k+1) = A\hat{x}_i(k) + Bu_i(k) + L_i(y_i(k) - C\hat{x}_i(k)) + \kappa_{\phi(k)} M_i \sum_{j=1}^{N} a_{ij}^{\phi(k)} (\hat{x}_j(k) - \hat{x}_i(k)), \tag{3}$$

where $\kappa_{\phi(k)}$ is the coupled gain that needs to be designed and M_i and L_i are observer gains of the ith subsystem, and $a_{ij}^{\phi(k)}$ represents the connectivity weight from subsystem i to subsystem j at moment k.

By subtracting (1) from (3), we obtain the error dynamics of a single subsystem:

$$\begin{aligned} e_i(k) &= x_i(k) - \hat{x}_i(k), \\ e_i(k+1) &= (A - L_i C)e_i(k) - \kappa_{\phi(k)} M_i \sum_{j=1}^{N} a_{ij}^{\phi(k)} (\hat{x}_j(k) - \hat{x}_i(k)) + D_i d_i(k), \end{aligned} \tag{4}$$

with $D_i = \begin{bmatrix} I & -L_i \end{bmatrix}$ and $d_i(k) = \begin{bmatrix} p_i(k) \\ q_i(k) \end{bmatrix}$.

Then we can obtain the dynamic system of the global observer

$$\begin{aligned} \hat{x}(k+1) = &\overline{A}\hat{x}(k) + \overline{B}u(k) + \overline{L}_{\phi(k)}(y(k) - \overline{C}\hat{x}(k)) \\ &+ \kappa_{\phi(k)} \overline{M}_{\phi(k)} (\mathcal{L}_{\phi(k)} \otimes I_N)(x(k) - \hat{x}(k)), \end{aligned} \tag{5}$$

with $\overline{L} = diag\{\underbrace{L_1, \cdots, L_N}_{N}\}$ and $\overline{M} = diag\{\underbrace{M_1, \cdots, M_N}_{N}\}$.

The global error system $e(k) = [e_1^T(k), \cdots, e_N^T(k)]^T$ is as follows

$$e(k+1) = (\overline{A} - \overline{L}_{\phi(k)}\overline{C} - \kappa_{\phi(k)}\overline{M}_{\phi(k)}(\mathcal{L}_{\phi(k)} \otimes I_N))e(k) + \overline{D}d(k), \tag{6}$$

and the compact form of (6) can be writen as

$$e(k+1) = \Gamma_{\phi(k)}e(k) + \overline{D}d(k), \tag{7}$$

where $\overline{D} = diag\{\underbrace{D_1, \cdots, D_N}_{N}\}$ and $\Gamma_{\phi(k)} = \overline{A} - \overline{L}_{\phi(k)}\overline{C} - \kappa_{\phi(k)}\overline{M}_{\phi(k)}(\mathcal{L}_{\phi(k)} \otimes I_N)$.

Definition 1 ([27])**.** *If the following condition holds,*

$$\|e(k)\|_2 \leq \varkappa\sqrt{\|d\|_\infty^2 + V(0)\omega^k}, \tag{8}$$

where $\varkappa > 0$ and $0 < \omega < 1$, $V(0) = e^T(0)P_{\phi(k)}e(0)$ and $P_{\phi(k)} \succ 0$. Then the observer (5) is a L_∞ robust observer for system (2).

Definition 2 ([28])**.** *Let $N_\psi(k_1, k_2)$ be the switching times of $\psi(k)$ across the range $[k_1, k_2)$. If*

$$N_\psi(k_1, k_2) \leq N_0 + \frac{k_2 - k_1}{\tilde{\tau}}, \tag{9}$$

for given $\tilde{\tau} > 0$ and $N_0 \geq 0$, $\tilde{\tau}$ is the average dwell time (ADT) of the switching signal $\psi(k)$. In this paper, we let $N_0 = 0$.

Definition 3 ([29])**.** *The definition of an α-dimensional zonotope is as follow*

$$\Omega = \nu \oplus HY^\alpha = \nu + Hz, z \in Y^\alpha, \tag{10}$$

where $\nu \in R^\iota$ represents a given vector, $H \in R^{\iota\times\alpha}$ represents a given matrix, Y^α is a unitary box made up of α unitary intervals and Y^α is a unitary interval. In the sequel, the zonotope Ω is represented as $\langle\nu, H\rangle$ for the sake of simplicity.

Lemma 3 ([30])**.** *The following equation is satisfied for a zonotope defined in (10):*

$$\begin{aligned}\langle\nu_1, H_1\rangle \oplus \langle\nu_2, H_2\rangle &= \langle\nu_1 + \nu_2, [H_1, H_2]\rangle,\\ W \odot \langle\nu, H\rangle &= \langle W\nu, WH\rangle,\\ \langle\nu, H\rangle &\subseteq \langle\nu, \overline{H}\rangle,\end{aligned}$$

where H_1 and H_2 represent the shape matrices of each of the zonotopes, and ν_1 and ν_2 are their centers. $\overline{H} \in R^{N\times N}$ means a diagonal matrix with $\overline{H}_{M,M} = \sum_{i=1}^{\alpha}|H_{M,i}|, M = 1, ..., \rho$.

Remark 1. *$\overline{H}$ can be expressed in the form shown below:*

$$\overline{H} = \begin{bmatrix}\sum_{i=1}^{\alpha}|H_{1,i}| & \cdots & 0\\ \vdots & \ddots & \vdots\\ 0 & \cdots & \sum_{i=1}^{\alpha}|H_{\rho,i}|\end{bmatrix}. \tag{11}$$

If $\alpha > \rho$, then $\langle\nu, H\rangle \subseteq \langle\nu, \overline{H}\rangle$ is applied to reduce the order of high order zonotopes.

Remark 2. *For zonotopes $\Omega_M \subset R^N, M = 1, ..., \rho$, the Minkowski sum of them is*

$$\bigoplus_{M=1}^{\rho} \Omega_M = \Omega_1 \oplus \Omega_2 \oplus \cdots \oplus \Omega_\rho. \tag{12}$$

Definition 4 ([19])**.** *For an α-order zonotope, there is an interval hull Ω that could contain Ω in its entirety:*

$$\Omega \subset Box(\Omega) = [a, b], \tag{13}$$

with $a = [a_1, \cdots, a_\alpha]^T$, $b = [b_1, \cdots, b_\alpha]^T$ and $Box(\cdot)$ stands for the interval hull. For any zonotope, the interval hull is the smallest interval vector.

Lemma 4 ([29])**.** *If $\Omega = \langle \nu, H \rangle$, the components of its interval hull are*

$$\begin{cases} a_i = \nu_i - \sum_{j=0}^{\alpha} |H_{ij}|, i = 1, \ldots, \iota, \\ b_i = \nu_i + \sum_{j=0}^{\alpha} |H_{ij}|, i = 1, \ldots, \iota. \end{cases} \tag{14}$$

Lemma 5 ([29])**.** *Given zonotopes Ω_i, $i = 1, 2, \ldots, m$*

$$Box(\bigoplus_{m=1}^{\rho} \Omega_m) = \bigoplus_{m=1}^{\rho} (Box(\Omega_m)). \tag{15}$$

Lemma 6 ([31])**.** *For the given symmetric matrix $\begin{bmatrix} \mathbb{A} & \mathbb{B} \\ \mathbb{B}^T & \mathbb{C} \end{bmatrix}$, the following inequalities are equivalent:*

(1) $\begin{bmatrix} \mathbb{A} & \mathbb{B} \\ \mathbb{B}^T & \mathbb{C} \end{bmatrix} \prec 0,$
(2) $\mathbb{C} \prec 0; \mathbb{A} - \mathbb{B}\mathbb{A}^{-1}\mathbb{B}^T \prec 0,$
(3) $\mathbb{A} \prec 0; \mathbb{C} - \mathbb{B}^T\mathbb{C}^{-1}\mathbb{B} \prec 0.$

Assumption 1. *The initial state of the ith subsystem satisfies the following condition*

$$\underline{x}_i(0) \leq x_i(0) \leq \overline{x}_i(0). \tag{16}$$

Assumption 2. *The disturbances and output noise in system* (6) *are bounded, which are:*

$$\|d(k)\|_2 \leq \|d\|_\infty, \tag{17}$$

where $\|d\|_\infty$ is a constant.

Assumption 3. *The initial state, disturbance and noise, and initial error are represented by $x(0)$, $d(0)$ and $e(0)$, which can be wrapped as in the equations below:*

$$\begin{aligned} x(0) &\in \langle \nu_0, H_0 \rangle = \mathcal{X}(0), \\ d(0) &\in \langle 0, E_d \rangle = \mathcal{D}(0), \\ e(0) &\in \langle 0, H_0 \rangle = \mathcal{E}(0), \end{aligned} \tag{18}$$

where H_0 is given matrix and $E_d = diag\{d_i\}$.

3. Main Results

In this part, we provide sufficient conditions for the observer with L_∞ property for CPS. Then, a reachability analysis methodology is used to design the distributed interval observer.

Theorem 1. *Let η and θ be two given constants with $0 < \eta < 1$ and $\theta > 1$. If there exists a constant χ and matrices $P_n \succ 0 \in R^{N\times N}$, $P_m \succ 0 \in R^{N\times N}$ such that*

$$\begin{cases} min \quad \chi^2, \\ subject \quad to: \\ \begin{bmatrix} -\eta P_n & * & * \\ 0 & -\chi^2 I_N & * \\ P_n\overline{A} - W_n\overline{C} - \kappa_n Q_n(\mathcal{L}_n \otimes I_N) & P_n\overline{D} & -P_n \end{bmatrix} \prec 0, \\ P_n \prec \theta P_m, \\ \frac{1}{\tilde{\tau}} + \frac{ln\eta}{ln\theta} < 0, \\ \kappa_n > \frac{1}{a(\mathcal{L}_n)}, \end{cases} \tag{19}$$

where $W_n = P_n\overline{L}_n, Q_n = P_n\overline{M}_n$, $n \neq m, \forall n, m \in S$ and $\tilde{\tau}$ satisfying ADT. Then (5) is a robust L_∞ observer for system (3).

Proof. Please see the Appendix A. □

Remark 3. *In Theorem 1, the parameter κ_n depends on $a(\mathcal{L}_n)$. The algebraic connectivity $a(\mathcal{L}_n)$ of a graph tends to increase with graph stability. As the stability of the graph increases, there will be a greater range of options for κ_n.*

Remark 4. *In practice, the ADT $\tilde{\tau}$ and the disturbance attenuation level χ^2 stand for the performance of the observer. Owing to the fact that the ADT $\frac{1}{\tilde{\tau}} + \frac{ln\eta}{ln\theta} < 0$ depends on η and θ, it is necessary to select suitable values for η and θ to minimize the ADT $\tilde{\tau}$.*

After completing the design of the optimal L_∞ observer, we need to construct the interval observer by designing the interval hull that can completely wrap the system disturbances, noise, and errors. The real-time error from (5) can be wrapped by the zonotope as

$$e(k) \in \langle v_0, H(k)\rangle = \mathcal{E}(k). \tag{20}$$

Then, we add the reachability analysis methodology to the distributed L_∞ observer designed in Theorem 1 and then give the following interval observer:

$$\begin{cases} \overline{x} = \hat{x} + \overline{e} \\ \underline{x} = \hat{x} + \underline{e} \end{cases} \tag{21}$$

where $\overline{e}$ and $\underline{e}$ are the upper and lower bounds of $e(k)$.

Theorem 2. *An interval estimate of the system state is provided by (22), if Assumption 3 holds, then the error $e(k)$ has the following upper and lower bounds:*

$$\left[\underline{e}(k), \quad \overline{e}(k)\right] = Box((\prod_{n=0}^{k-1} \Gamma_n)\mathcal{E}(0)) \oplus \bigoplus_{n=0}^{k-1} Box((\prod_{m=1}^{k-1} \Gamma_m)\Gamma_n^{-1} D\mathcal{D}), \tag{22}$$

where $Box(\mathcal{E}(0)) = \left[\underline{e}(0), \quad \overline{e}(0)\right]$.

Proof. Based on Assumption 3, we can obtain $\mathcal{E}(1)$,

$$\mathcal{E}(1) = \Gamma_{\phi(0)}\mathcal{E}(0) \oplus D\mathcal{D}. \tag{23}$$

When $k = 1$, then we can obtain

$$\begin{aligned} \mathcal{E}(2) &= \Gamma_{\phi(1)}\mathcal{E}(1) \oplus D\mathcal{D} \\ &= \Gamma_{\phi(1)}\Gamma_{\phi(0)}\mathcal{E}(0) \oplus \Gamma_{\phi(1)}D\mathcal{D} \oplus D\mathcal{D}. \end{aligned} \tag{24}$$

Iterating the above process yields

$$\mathcal{E}(k+1) = (\prod_{n=0}^{k-1} \Gamma_n)\mathcal{E}(0) \oplus \bigoplus_{n=0}^{k-1} (\prod_{m=1}^{k-1} \Gamma_m)\Gamma_n^{-1} D\mathcal{D}. \tag{25}$$

Then the interval hull below describes the set $\mathcal{E}(k)$

$$\mathcal{E}(k) = [\underline{e}(k), \quad \overline{e}(k)] = Box((\prod_{n=0}^{k-1} \Gamma_n)\mathcal{E}(0)) \oplus \bigoplus_{n=0}^{k-1} Box((\prod_{m=1}^{k-1} \Gamma_m)\Gamma_n^{-1} D\mathcal{D}). \tag{26}$$

□

The proof of Theorem 2 is now completed.

Based on Theorems 1 and 2, the design of a distributed interval observer with switching topology can be implemented by Algorithm 1.

Remark 5. *According to Theorem 1, the robust L_∞ observer is designed to reduce the effect of outside disturbance and output noise. It is obvious that a bounded interval hull exists based on the result of Theorem 1, which can include errors and disturbances. Then, using the given interval hull $\mathcal{E}(0)$ as a starting point, Theorem 2 gives the interval hull $\mathcal{E}(k)$. We propose a reachable set analysis technique by combining Theorem 1 with Theorem 2.*

Algorithm 1: Algorithm for designing the distributed interval observer with switching topology.

(1) Model CPSs with given disturbances and noise.
(2) Design distributed observers for subsystems.
(3) Select the appropriate κ_n according to the switching topology.
(4) Solve the LMI problem in Theorem 1 using the information of the bounds of disturbances
and noise.
(5) Calculate the gains of the observers by $\overline{M}_n = P_n^{-1}Q_n, \overline{L}_n = P_n^{-1}W_n$.
(6) Determine the ADT by given η and θ.
(7) Obtain the zonotopes of the initial value according to (18)
(8) Transform the zonotope at the moment $k = n$ into an interval hull starting from $n = 0$.
(9) Iterate the interval hull in step (6).
(10) Obtain the interval hull at the moment $k = n + 1$.
(11) The interval observer is obtained through (21).

Remark 6. *If the modeling uncertainty is taken into consideration, the new model of this paper is as follows:*

$$\begin{aligned} x_i(k+1) &= (A + \Delta A(k))x_i(k) + (B + \Delta B(k))u_i(k) + p_i(k), \\ y_i(k) &= (C + \Delta C(k))x_i(k) + q_i(k), \end{aligned}$$

where $\Delta A(k), \Delta B(k)$ and $\Delta C(k)$ represent the uncertainty of the system, respectively. Then, we may use the norm-bounded condition on $\Delta A(k), \Delta B(k)$ and $\Delta C(k)$ to design the L_∞ interval observer. However, it is not an easy task to construct the interval hull of the corresponding error system since *the time-varying terms are contained. In the near future, we will deal with systems with model uncertainty with the method proposed in this paper.*

Remark 7. *In Theorems 1 and 2, limited by the current knowledge of authors, this paper only gives sufficient conditions for observer design. In the future, we will study the necessary conditions for the design of interval observers, and in conjunction with this paper, we will give the necessary and sufficient conditions for the design of interval observers.*

4. Simulation

Among CPSs, UAVs have recently achieved widespread application. In this section, we simulate through a networked CPSs with four UAVs.

Referring to [11], the dynamical system of each UAV is as follows

$$\begin{aligned} \begin{bmatrix} \dot{\alpha}_i(t) \\ \dot{\beta}_i(t) \end{bmatrix} &= A \begin{bmatrix} \alpha_i(t) \\ \beta_i(t) \end{bmatrix} + Bu_i(k) + p_i(k), \\ y_i(k) &= C \begin{bmatrix} \alpha_i(t) \\ \beta_i(t) \end{bmatrix} + q_i(k), \end{aligned} \tag{27}$$

where the pitch rate and angle of attack of each UAV are indicated by $\beta_i(t)$ and $\alpha_i(t)$. The schematic of each UAV is shown in Figure 1, and the detailed derivation of the dynamics model is omitted here.

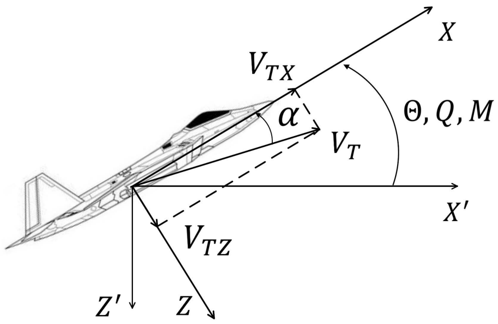

Figure 1. Longitudinal axis system of UAV.

Table 1 displays the output noise and the external disturbance borrowed from [11], and the partial matrix values are as follows:

$$A = \begin{bmatrix} 0.8825 & 0.0987 \\ -0.8458 & 0.9122 \end{bmatrix}, B = \begin{bmatrix} -0.0194 & -0.0036 \\ -1.9290 & -0.3803 \end{bmatrix}, C = \begin{bmatrix} 1 & 0.2 \end{bmatrix}.$$

Table 1. The output noise and the external disturbance.

Subsystem	Output Noise	External Disturbance
1	$0.1\cos(k)$	$0.2 + 0.1\cos(0.5k)$
2	$0.1\sin(k)$	$0.1\cos(0.1k)$
3	$0.01\cos(k)$	$\cos(0.2\pi k) + 0.3\sin(0.2\pi k)$
4	$0.05\sin(k)$	$\cos(0.3\pi k) + 0.1\sin(0.3\pi k)$

For illustrative purposes, Figure 2 shows a switching communication topology $\mathcal{G}_1$,$\mathcal{G}_2$ and $\mathcal{G}_3$ with four UAVs. Figure 3 displays the change in the switching signal $\phi(k)$. Then, from Figure 2, we can give the corresponding matrix $\mathcal{L}_n$:

$$\mathcal{L}_1 = \begin{bmatrix} 1 & -1 & 0 & 0 \\ -1 & 3 & -1 & -1 \\ 0 & -1 & 2 & -1 \\ 0 & -1 & -1 & 2 \end{bmatrix}, \mathcal{L}_2 = \begin{bmatrix} 1 & -1 & 0 & 0 \\ 0 & 2 & -1 & -1 \\ 0 & 0 & 1 & -1 \\ -1 & -1 & 0 & 2 \end{bmatrix}, \mathcal{L}_3 = \begin{bmatrix} 1 & 0 & 0 & -1 \\ 0 & 1 & 0 & -1 \\ 0 & 0 & 1 & -1 \\ -1 & -1 & -1 & 3 \end{bmatrix}.$$

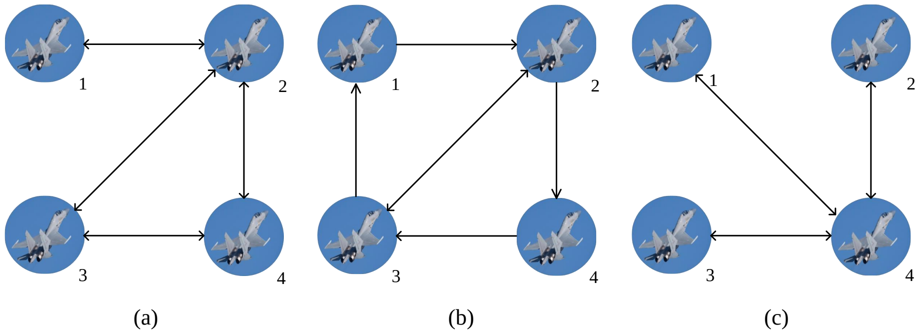

Figure 2. Three switching communication topology of UAVs.

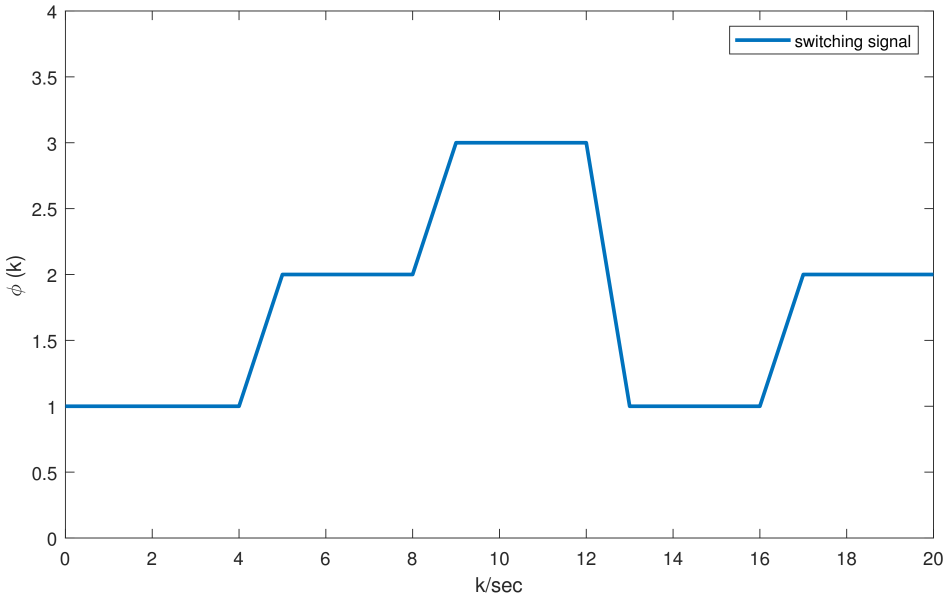

Figure 3. The change in the switching signal of distributed interval observers.

From Lemmas 1 and 2, we can obtain $a(\mathcal{L}_1) = a(\mathcal{L}_2) = a(\mathcal{L}_3) = 1$, then we have $\kappa > 1$. In this simulation, $\kappa_1 = 1.8, \kappa_2 = 2.3, \kappa_3 = 3.2$ are chosen. We can determine L_n and M_n by solving (19), the observer gains for 1th subsystem are listed below

$$L_1 = \begin{bmatrix} 47.8095 & -46.2386 \end{bmatrix}, L_2 = \begin{bmatrix} -9.5528 & 47.7273 \end{bmatrix}, L_3 = \begin{bmatrix} 17.8244 & -11.9289 \end{bmatrix}.$$

$$M_1 = \begin{bmatrix} -41.7480 & -36.5506 \\ -1.8874 & -6.9585 \end{bmatrix}, M_2 = \begin{bmatrix} 10.3302 & 8.4984 \\ -79.5140 & -71.1991 \end{bmatrix}, M_3 = \begin{bmatrix} -11.7589 & -7.5478 \\ -6.1219 & -9.0834 \end{bmatrix}.$$

The peak estimation error of Angle of Attack and Pitch Rate of 1th subsystem are 0.4184 and 0.7668, respectively. The disturbance attenuation level χ^2 and ADT $\tilde{\tau}$ are as follows

$$\chi^2 = 0.4984, \tilde{\tau} \leq 0.1763.$$

Below are the results of the numerical simulation. The states of the original systems and the upper and lower observers are depicted in Figures 4 and 5. x_{ij} are the original states of the subsystems. u_{ij} and v_{ij} reflect the bounds produced via the interval hull technique used in this paper and the monotone system method in [32], where i denotes the ith subsystem and j denotes the jth state. Figure 6 shows the error system for a single subsystem, eu_{ij}, and ev_{ij} reflect the observation error through the method used in this paper and the monotone system method in [32].

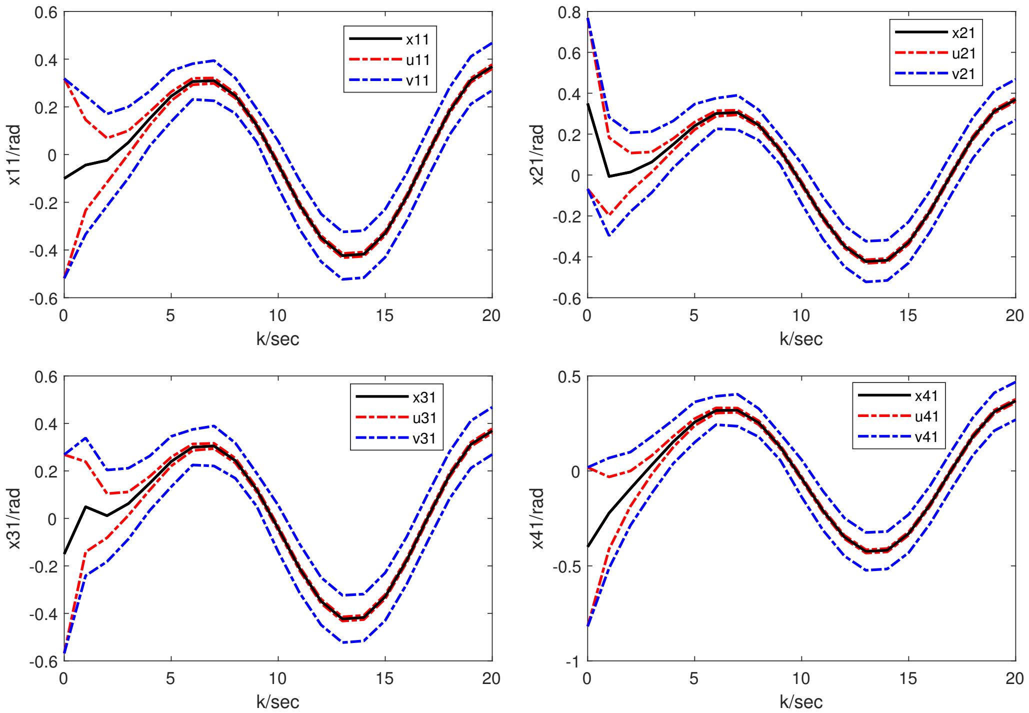

Figure 4. Angle of attack and interval estimates of UAVs.

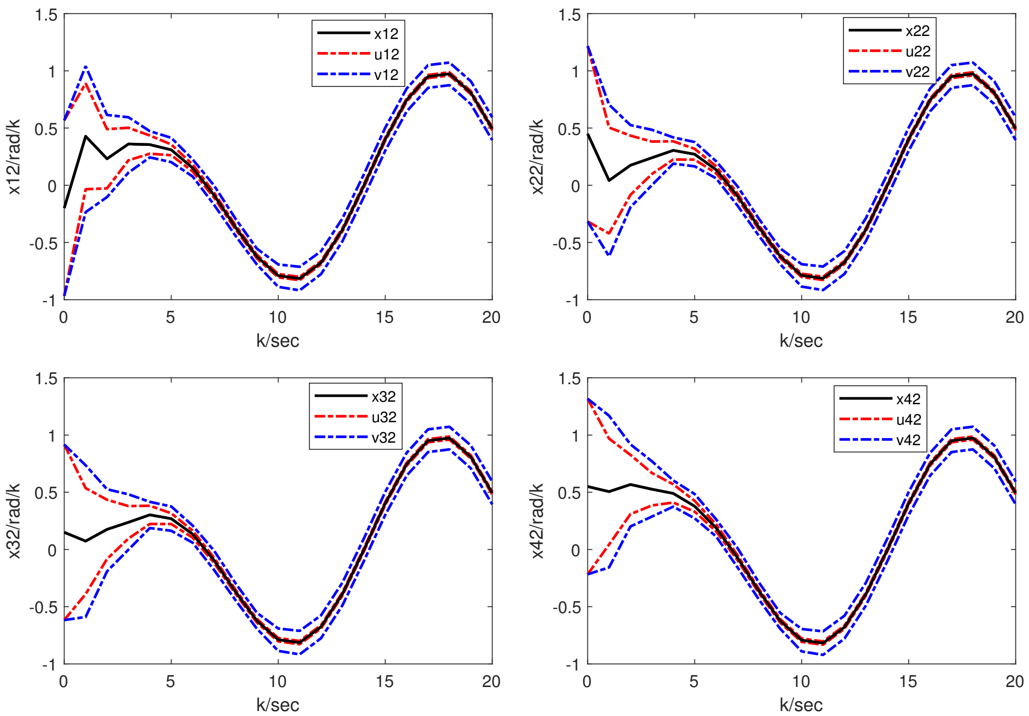

Figure 5. Pitch rate and interval estimates of UAVs.

It is evident that the states of CPS are completely surrounded by those of the upper and lower observers. From Figures 4–6, it can be seen that the distributed interval observer designed in this paper has higher estimation accuracy compared to the traditional monotone system approach in [32]. We design the optimal robust observer using the L_∞ technique, which reduces the design requirements of the observer, unlike the H_∞ technique applied in [24]. Different from [23] and most of the work, we consider for the first time the case of switching topology among distributed interval observers. Thus, the proposed distributed interval observers design method for CPSs is effective and feasible.

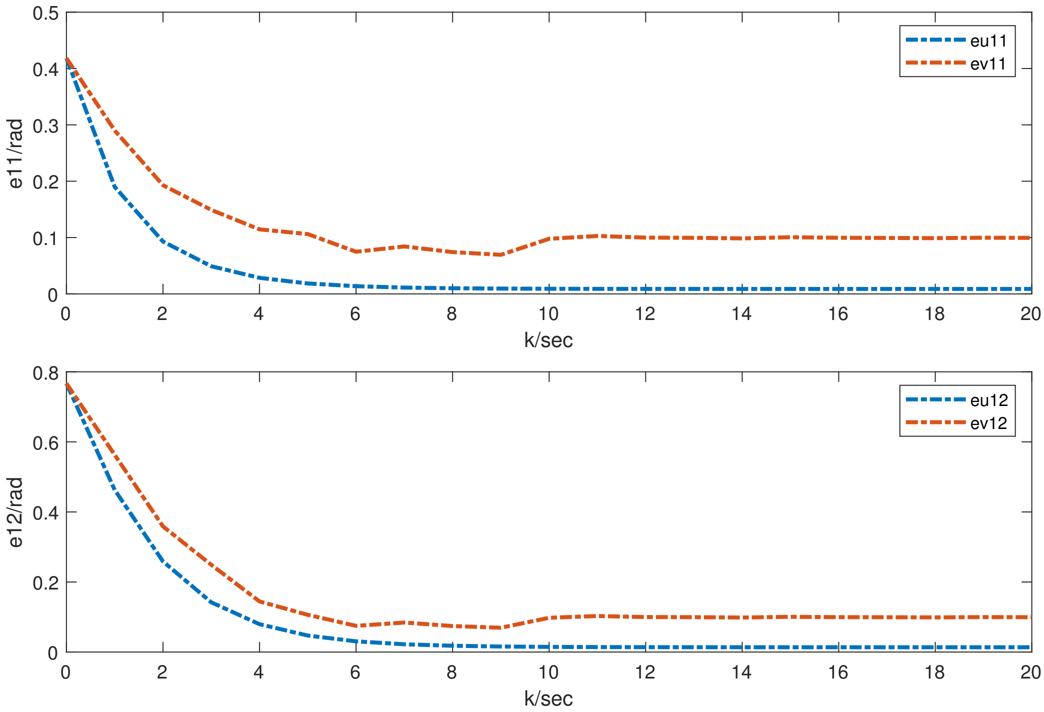

Figure 6. Observation error of angle of attack and pitch rate of UAVs.

Remark 8. *For networked CPSs with perturbations and noise, we propose a class of distributed interval observer design methods with switching topology that combine the design of L_∞ observers with interval hulls. This class of methods eliminates the need to consider the error system to be Schur and, therefore, eliminates the need to use coordinate transformation methods, significantly reducing the conservatism of the estimation. It can be seen from the observer form* (3)*, sufficient conditions* (19)*, and the proof of Theorem 1. In addition, the estimation accuracy is better than that in [32], as it can also be seen from* (22)*.*

5. Conclusions

In this paper, a distributed interval estimation method for uncertain CPSs is investigated. Due to the communication burden of networked CPSs, we consider the case of switching topology among distributed interval observers. To improve the accuracy of the estimation, a reachability analysis is introduced in conjunction with the L_∞ technique. Finally, the validity of the main results of this paper is verified by one example. In the future, we may focus our research on the distributed interval estimation of the attacked CPSs.

Author Contributions: Methodology, J.Z.; validation, C.L.; writing—original draft preparation, J.Z.; writing—review and editing, J.H.; supervision, J.H. All authors have read and agreed to the published version of the manuscript.

Funding: This research received no external funding.

Data Availability Statement: Data are contained within the article.

Conflicts of Interest: The authors declare no conflict of interest.

Appendix A

Proof. Define $\mathcal{A} = \begin{bmatrix} -\eta P_n & 0 \\ 0 & -\chi^2 I_N \end{bmatrix}$, $\mathcal{B} = \begin{bmatrix} P_n\overline{A} - W_n\overline{C} - \kappa_n Q_n(\mathcal{L}_n \otimes I_N) \\ P_n\overline{D} \end{bmatrix}$, $\mathcal{C} = -P_n$. Using Lemma 6 and the fact that $\mathcal{C} \prec 0$, we can determine that

$$\mathcal{A} - \mathcal{B}\mathcal{A}^{-1}\mathcal{B}^T \prec 0. \tag{A1}$$

Substituting $Q_n = P_n\overline{M}_n, W_n = P_n\overline{L}_n$ into (5), we obtain

$$G = \begin{bmatrix} \Gamma_n^T P_n \Gamma_n - \eta P_n & * \\ \overline{D}^T P_n \Gamma_n & \overline{D}^T P_n \overline{D} - \chi^2 I_N \end{bmatrix} \prec 0. \tag{A2}$$

where $\Gamma_n = \overline{A} - \overline{L}_n\overline{C} - \kappa_n\overline{M}_n(\mathcal{L}_n \otimes I_N)$. It follows from (A2) that

$$\begin{bmatrix} e^T(k) & d^T(k) \end{bmatrix} \begin{bmatrix} \Gamma_n^T P_n \Gamma_n - \eta P_n & * \\ \overline{D}^T P_n \Gamma_n & \overline{D}^T P_n \overline{D} - \chi^2 I_N \end{bmatrix} \begin{bmatrix} e(k) \\ d(k) \end{bmatrix} \prec 0. \tag{A3}$$

Thus, (A3) implies that

$$e^T(k)(\Gamma_n^T P_n \Gamma_n - \eta P_n)e(k) + d^T(k)(\overline{D}^T P_n \overline{D} - \chi^2 I_N)d(k) + 2d^T(k)\overline{D}^T P_n \Gamma_n e(k) < 0. \tag{A4}$$

We then choose the following Lyapunov function

$$V_n(k) = e^T(k)P_n e(k). \tag{A5}$$

Thus,

$$\begin{aligned} \triangle V_n(k) =& V_n(k+1) - V_n(k) \\ =& e^T(k)(\Gamma_n^T P_n \Gamma_n - \eta P_n)e(k) + d^T(k)(\overline{D}^T P_n \overline{D} - \chi^2 I_N)d(k) \\ &+ 2d^T(k)\overline{D}^T P_n \Gamma_n e(k). \end{aligned} \tag{A6}$$

Further simplification of (A6) yields

$$\triangle V_n(k) < (\eta - 1)e^T(k)P_n e(k) + \chi^2 d^T(k)d(k), \tag{A7}$$

which means

$$V_n(k+1) < \eta V_n(k) + \chi^2 d^T(k)d(k). \tag{A8}$$

Then consider the interval $[k_\sigma, k)$. Iterating (A8) yields

$$V_n(k) < \eta^{k-k_\sigma} V_n(k_\sigma) + \chi^2 \sum_{\varrho=0}^{k-k_\sigma-1} \eta^\varrho d^T(k-1-\varrho)d(k-1-\varrho). \tag{A9}$$

Suppose that $\phi(k_{\sigma-1}) = m$, using $P_n \prec \theta P_m$, then

$$\begin{aligned} V_n(k) <& \eta^{k-k_\sigma} V_n(k_\sigma) + \chi^2 \sum_{\varrho=0}^{k-k_\sigma-1} \eta^\varrho d^T(k-1-\varrho)d(k-1-\varrho) \\ <& \eta^{k-k_\sigma+1}\theta V_m(k_\sigma - 1) + \eta^{k-k_\sigma}\theta\chi^2 d^T(k_\sigma - 1)d(k_\sigma - 1) \\ &+ \chi^2 \sum_{\varrho=0}^{k-k_\sigma-1} \eta^l d^T(k-1-\varrho)d(k-1-\varrho). \end{aligned} \tag{A10}$$

Iterating (A10) yields the inequality below

$$V_n(k) < \eta^k \theta^{N_\phi(0,k)} V_{\phi(0)}(0) + \chi^2 \sum_{\varrho=0}^{k-k_\sigma-1} \eta^\varrho \theta^{N_\phi(k-\varrho,k)} d^T(k-1-\varrho) d(k-1-\varrho). \tag{A11}$$

In view of $\theta > 1$ and $N_\phi(0,k) \geq N_\phi(k-\varrho,k)$, we have

$$\begin{aligned} &\chi^2 \sum_{\varrho=0}^{k-k_\sigma-1} \eta^\varrho \theta^{N_\phi(k-\varrho,k)} d^T(k-1-\varrho) d(k-1-\varrho) \\ &< \chi^2 \sum_{\varrho=0}^{k-k_\sigma-1} \eta^\varrho \theta^{N_\phi(0,k)} d^T(k-1-\varrho) d(k-1-\varrho). \end{aligned} \tag{A12}$$

It follows from (A11) and (A12) that

$$V_n(k) < \theta^{N_\phi(0,k)} [\eta^k V_{\phi(0)}(0) + \chi^2 \sum_{\varrho=0}^{k-k_\sigma-1} \eta^l d^T(k-1-\varrho) d(k-1-\varrho)]. \tag{A13}$$

Due to $V_n(k) \geq \underline{\lambda} \|e(k)\|_2^2$, the error $e(k)$ in (6) satisfies

$$\begin{aligned} &\|e(k)\|_2^2 \leq \frac{1}{\underline{\lambda}(P_n)} V_n(k), \\ &\|e(k)\|_2^2 \leq \frac{\theta^{N_\phi(0,k)}}{\underline{\lambda}(P_n)} (\eta^k V_{\phi(0)}(0) + \chi^2 \sum_{\varrho=0}^{k-1} \eta^\varrho \|d(k)\|_\infty^2). \end{aligned} \tag{A14}$$

By Definition 1, the proof of Theorem 1 is completed. □

References

1. Cao, X.; Cheng, P.; Chen, J.; Sun, Y. An online optimization approach for control and communication codesign in networked cyber-physical systems. *IEEE Trans. Ind. Inform.* **2012**, *9*, 439–450. [CrossRef]
2. Gunes, V.; Peter, S.; Givargis, T.; Vahid, F. A survey on concepts, applications, and challenges in cyber-physical systems. *KSII Trans. Internet Inf. Syst.* **2014**, *8*, 4242–4268.
3. Kim, K.D.; Kumar, P.R. Cyber–physical systems: A perspective at the centennial. *Proc. IEEE* **2012**, *100*, 1287–1308.
4. Cai, S.; Lau, V.K. Zero MAC latency sensor networking for cyber-physical systems. *IEEE Trans. Signal Process.* **2018**, *66*, 3814–3823. [CrossRef]
5. Sangaiah, A.K.; Siarry, P. Cognitive Brain-Inspired Cyber-Physical Systems in Industrial Informatics. *Front. Neurorobot.* **2022**, *16*, 926538. [CrossRef]
6. Mitchell, R.; Chen, R. Modeling and analysis of attacks and counter defense mechanisms for cyber physical systems. *IEEE Trans. Reliab.* **2015**, *65*, 350–358. [CrossRef]
7. Verma, R. Smart city healthcare cyber physical system: Characteristics, technologies and challenges. *Wirel. Pers. Commun.* **2022**, *122*, 1413–1433. [CrossRef]
8. Hozdić, E.; Butala, P. Concept of socio-cyber-physical work systems for Industry 4.0. *Tehnički Vjesn.* **2020**, *27*, 399–410.
9. Wu, C.; Hu, Z.; Liu, J.; Wu, L. Secure estimation for cyber-physical systems via sliding mode. *IEEE Trans. Cybern.* **2018**, *48*, 3420–3431. [CrossRef]
10. Chang, Y.H.; Hu, Q.; Tomlin, C.J. Secure estimation based Kalman filter for cyber–physical systems against sensor attacks. *Automatica* **2018**, *95*, 399–412. [CrossRef]
11. Zhang, C.L.; Yang, G.H.; Lu, A.Y. Resilient observer-based control for cyber-physical systems under denial-of-service attacks. *Inf. Sci.* **2021**, *545*, 102–117. [CrossRef]
12. Gouzé, J.L.; Rapaport, A.; Hadj-Sadok, M.Z. Interval observers for uncertain biological systems. *Ecol. Model.* **2000**, *133*, 45–56. [CrossRef]
13. Raïssi, T.; Efimov, D.; Zolghadri, A. Interval state estimation for a class of nonlinear systems. *IEEE Trans. Autom. Control* **2011**, *57*, 260–265. [CrossRef]
14. Mazenc, F.; Dinh, T.N.; Niculescu, S.I. Interval observers for discrete-time systems. *Int. J. Robust Nonlinear Control* **2014**, *24*, 2867–2890. [CrossRef]
15. Tang, W.; Wang, Z.; Wang, Y.; Raïssi, T.; Shen, Y. Interval estimation methods for discrete-time linear time-invariant systems. *IEEE Trans. Autom. Control* **2019**, *64*, 4717–4724. [CrossRef]

16. Zhou, X.; Wang, Z.; Wang, J. Automated Ground Vehicle Path-Following: A Robust Energy-to-Peak Control Approach. *IEEE Trans. Intell. Transp. Syst.* **2022**, *23*, 14294–14305. [CrossRef]
17. Zhang, W.; Chen, Y.; Gao, H. Energy-to-peak control for seismic-excited buildings with actuator faults and parameter uncertainties. *J. Sound Vib.* **2011**, *330*, 581–602. [CrossRef]
18. Feng, J.; Han, K. Robust full- and reduced-order energy-to-peak filtering for discrete-time uncertain linear systems. *Signal Process.* **2015**, *108*, 183–194. [CrossRef]
19. Huang, J.; Che, H.; Raïssi, T.; Wang, Z. Functional interval observer for discrete-time switched descriptor systems. *IEEE Trans. Autom. Control* **2021**, *67*, 2497–2504. [CrossRef]
20. Guo, S.; Ren, W.; Ahn, C.K.; Wen, C.; Lam, H.K. Reachability analysis-based interval estimation for discrete-time Takagi–Sugeno fuzzy systems. *IEEE Trans. Fuzzy Syst.* **2021**, *30*, 1981–1992. [CrossRef]
21. Ren, W.; Guo, S. State and Faults Interval Estimations for Discrete-time Linear Systems. *Int. J. Control Autom. Syst.* **2023**, *21*, 2303–2312. [CrossRef]
22. Zhang, Z.H.; Yang, G.H. Distributed fault detection and isolation for multiagent systems: An interval observer approach. *IEEE Trans. Syst. Man Cybern. Syst.* **2018**, *50*, 2220–2230. [CrossRef]
23. Li, D.; Chang, J.; Chen, W.; Raïssi, T. IPR-based distributed interval observers design for uncertain LTI systems. *ISA Trans.* **2022**, *121*, 147–155. [CrossRef] [PubMed]
24. Huang, J.; Zhang, H.; Raïssi, T. Distributed interval estimation methods for multiagent systems. *IEEE Syst. J.* **2022**, *17*, 1843–1852. [CrossRef]
25. Yu, W.; Chen, G.; Cao, M.; Kurths, J. Second-order consensus for multiagent systems with directed topologies and nonlinear dynamics. *IEEE Trans. Syst. Man Cybern. Part B (Cybern.)* **2009**, *40*, 881–891.
26. Li, Z.; Liu, X.; Fu, M.; Xie, L. Global H_∞ consensus of multi-agent systems with Lipschitz non-linear dynamics. *IET Control Theory Appl.* **2012**, *6*, 2041–2048. [CrossRef]
27. Briat, C. Robust stability and stabilization of uncertain linear positive systems via integral linear constraints: L1-gain and L_∞-gain characterization. *Int. J. Robust Nonlinear Control* **2013**, *23*, 1932–1954. [CrossRef]
28. Zhao, X.; Zhang, L.; Shi, P.; Liu, M. Stability of switched positive linear systems with average dwell time switching. *Automatica* **2012**, *48*, 1132–1137. [CrossRef]
29. Alamo, T.; Bravo, J.M.; Camacho, E.F. Guaranteed state estimation by zonotopes. *Automatica* **2005**, *41*, 1035–1043. [CrossRef]
30. Combastel, C. Zonotopes and Kalman observers: Gain optimality under distinct uncertainty paradigms and robust convergence. *Automatica* **2015**, *55*, 265–273. [CrossRef]
31. Boyd, S.; El Ghaoui, L.; Feron, E.; Balakrishnan, V. *Linear Matrix Inequalities in System and Control Theory*; SIAM: Philadelphia, PA, USA, 1994.
32. Zhang, H.; Huang, J.; He, S. Fractional-order interval observer for multiagent nonlinear systems. *Fractal Fract.* **2022**, *6*, 355. [CrossRef]